

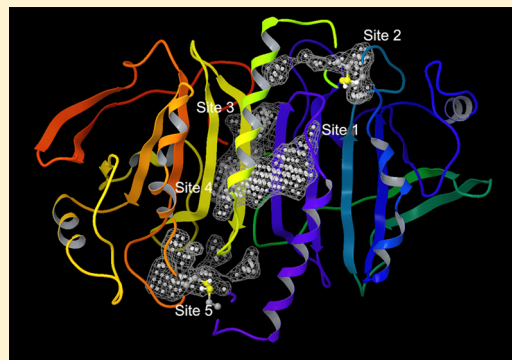
Elucidation of Allosteric Inhibition Mechanism of 2-Cys Human Peroxiredoxin by Molecular Modeling

Minsup Kim,[†] Keun Woo Lee,[‡] and Art E. Cho^{*†}

[†]Department of Bioinformatics, Korea University, Sejong, Korea

[‡]Division of Applied Life Science (BK21 Program), Research Institute of Natural Science (RINS), Plant Molecular Biology and Biotechnology Research Center (PMBBRC), Gyeongsang National University, Gazwa-dong, Jinju, Korea

ABSTRACT: We used molecular dynamics (MD) simulations and protein docking to elucidate the mechanism of allosteric inhibition of the human form of peroxiredoxin (Prx), 2-Cys proliferation associated gene (PAG). Beginning by using the rat form of Prx, 2-Cys heme-binding protein as a template, we used homology modeling to find the structure of human 2-Cys PAG, which is in dimeric form. Molecular dynamics simulations showed that the structure of the reduced form of the 2-Cys PAG dimer fluctuates as the two monomers drift away and approach each other. We then used SiteMap to search for binding sites on the surface of this dimer. A binding site between the two monomers was found, and virtual screening with docking was performed to identify a ligand binding to this site. Subsequent MD simulation revealed that with this ligand in the binding site, the dimer structure of 2-Cys PAG becomes stabilized such that two cysteine residues from two monomers, which are partners of a disulfide bond of the oxidized form, remain separated. This mechanism can be used as an allosteric inhibition of Prx as a hydrogen peroxide reducer, the role of which has been studied as an anticancer drug target.



INTRODUCTION

Sometimes called an “oxidation storm in the cell,” oxidative stress is a process by which active oxygen atoms, such as those in hydrogen peroxide (H_2O_2), are created and diffused rapidly throughout the cell, randomly damaging most biomolecules, including DNA and RNA. To prevent such cellular damage, living organisms fortify themselves with antioxidative enzymes as a defense mechanism. In particular, mammals are endowed with various kinds of peroxidases, which can reduce H_2O_2 to water.^{1–3} Peroxidases can be divided broadly into catalase, glutathione peroxidase (Gpx), and peroxiredoxin (Prx). Of these, Prx effectively controls the levels of cytokine-induced peroxide.^{3–5} Recent research has shown that Prx can defend oxidative stress reactions, such as cell-growth arrest and apoptosis, assigning both tasks of peroxide control and defense against oxidative stress.⁶ Based on the number and structure of cysteine residues involved in the reaction and mechanistic data, Prx can be classified into typical 2-Cys Prx, atypical 2-Cys Prx, and 1-Cys Prx.^{7–9} Typical 2-Cys Prx is the largest class in the Prx family and can be further divided according to its two redox active cysteines: the peroxidatic cysteine (generally, near residue 50) and the resolving cysteine (near residue 170). Typical 2-Cys Prx exists as a homodimer structure and thus possesses two active sites with redox-active cysteines.^{10,11} Typical 2-Cys Prx reaction consists of two steps revolving around the redox-active cysteine, which is called peroxidatic cysteine (Figure 1). In the first step of this reaction, the peroxidatic cysteine (Cys-SpH) attacks the peroxide substrate and is oxidized into cysteine sulfenic acid (Cys-SOH). The

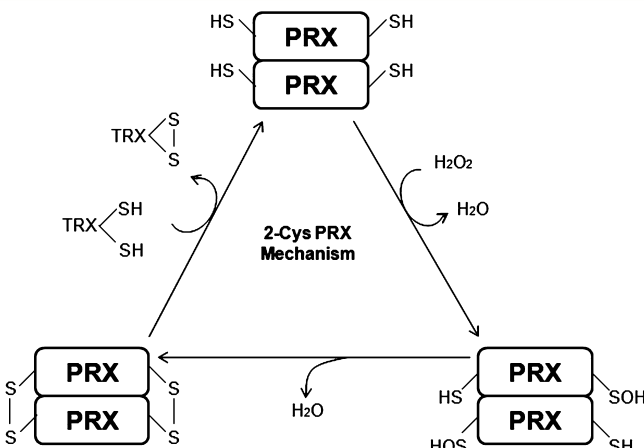


Figure 1. Redox cycle of Prx.

second step is the peroxidase reaction, in which one subunit of the peroxidatic cysteine sulfenic acid (Cys-SpOH) is attacked by resolving the cysteine that exists at the C-terminus of other subunit.³ This condensation reaction results in the formation of a stable intersubunit disulfide bond, which is then reduced by one of several cell-specific disulfide oxidoreductases (e.g., thioredoxin, AhpF, tryparedoxin, or AhpD), completing the catalytic cycle.^{12–14}

Received: September 19, 2012

Published: November 29, 2012

It has been found that several oncogenes are induced by reactive oxygen species (ROS).¹⁵ This fact confirms that it is necessary for cancer cells to acquire adaptive mechanisms to tolerate high redox levels. One such mechanism is the increased expression of Prx in cancer cells.^{16,17} Several studies have shown that ablation of various forms of Prx renders cancer cells sensitive to ROS-induced apoptosis;^{18,19} therefore, it has been suggested that disturbing this cycle of Prx, thereby inhibiting its function as a reducing agent for H₂O₂, can result in death of the cancerous cell.^{20,21} For this reason, Prx has been studied as an anticancer target.

Finding inhibitors of a target protein is the main objective of a drug discovery program. In searching for a compound that can inhibit the function of a protein, the right binding site on the protein must be found for that compound, and there could be more than one such binding site. It has recently become important to look into those binding sites, which are not the ones to which native ligands bind. If binding to these sites inhibits native ligand binding, it is known as "allosteric inhibition." Allosteric inhibition has several advantages over competitive inhibition. For example, because an allosteric site can be more diverse than the active site, whose structure is more preserved through evolution processes, targeting allosteric site would bring better specificity.^{22,23}

In this paper, we describe a process in which an allosteric binding site on human Prx is identified through molecular modeling and show how it can lead to the discovery of an allosteric inhibition mechanism.

METHODS

Choice of Structure File. The target protein of this study belongs to one of the six subclasses of mammalian Prx called "proliferation-associated gene product" (PAG), which is Prx subclass 1. It has been shown that Prx 1 is the most expressed Prx subclass in human cells and is the major peroxide reducer;²⁴ therefore, we restricted ourselves to Prx 1 in our experiment. Although there are a number of solved structures of human Prx of other subclasses, to this date, there is no human Prx 1 structure in the Protein Data Bank (PDB); therefore, it is necessary to perform homology modeling to obtain the target protein structure. For the template structure, a human Prx structure such as natural killer enhancing factor-B (NFEF-B; PDB ID: 1QMV), which is of subclass 2, could be used; however, since it is a paralog of Prx 1, the sequence identity rate of this protein to human PAG is lower than that of certain orthologs. In particular, human PAG and rat heme-binding protein (HBP) have a 96% sequence identity rate; whereas human PAG and human NFEF-B have 76%. Therefore, in this study, we used HBP23, which is the rat HBP.

Structure Prediction. The PDB ID for RN-Prx (HBP23)^{10,25,26} is 1QQ2. The amino acid sequence (ID CAA48137) of PAG was obtained through the NCBI Web site. With the sequence identity rate being as high as 96%, it is almost certain that homology modeling would yield a usable structure. We performed homology modeling using SWISS-MODEL server²⁷ (Automated Comparative Protein Modeling Server, version 8.05, GlaxoWellcome Experimental Research, Geneva, Switzerland), available through the European Bioinformatics Institute (EBI) Web site (<http://www.ebi.ac.kr/swiss-model>).

Binding Site Prediction. Although the active site of 2-Cys Prx is known, in order to scan for more efficient binding sites, we used a binding site prediction tool called "SiteMap"

(Schrödinger Inc., Portland, OR, U.S.A.). SiteMap^{28,29} searches the surface of a protein for possible binding sites and scores them according to size, degrees of enclosure and exposure, tightness, hydrophobic and hydrophilic character, and physical descriptors of hydrogen-bond donors and acceptors. We ran SiteMap on the predicted structure of human Prx coming from homology modeling. When an estimation of the volume of discovered binding sites was needed, the volume measurement option of SiteMap was used.

Molecular Dynamics Simulation. We performed molecular dynamics (MD) simulation to check the change in the structure of the binding site and active site. In this work, all the MD simulations were carried out with Desmond 2.26 (DESRES) and analyzed with Maestro's trajectory visualizer. For each MD simulation, we began with Desmond model builder. The cell size was approximately 51.7 × 70.1 × 53.8 Å, and the shape was orthorhombic. The water molecules were modeled with TIP3P. Ion neutralizer option was selected to balance the charge of the system. After a short minimization step and equilibration run, the main MD simulation was performed. We used the NVT ensemble with the Nose–Hoover thermostat method set at a reference temperature of 300 K. The time step was set at 2 fs, the default value of the Desmond program. Desmond uses, by default, a cutoff distance of 9 Å and Ewald summation for long-range Coulombic interactions. OPLS2005 force field was used for all simulations.

Virtual Screening. We relied on a virtual screening process to find a ligand that could act as an inhibitor to the allosteric binding site we investigated. For this, we used a docking method with Glide 5.5 (Schrödinger Inc.). Glide is based on grids for energy scoring and ligand matching. One starts with receptor grid generation, in which a grid is generated that conforms to the shape and properties of the receptor. Conformational search in Glide is done in a hierarchical way. Rough matching of ligand atom positions and grid points generates a set of possible ligand poses, which are refined through a successive optimization procedure. At the end of the process, ligand poses are scored with GlideScore and ranked accordingly. ZINC,³⁰ a database of small molecules, was used for drug-like compounds screening.

RESULTS AND DISCUSSION

Structure of Human PAG. By performing homology modeling with 2-Cys Prx HBP as a template, we obtained a 3-D structure prediction of 2-Cys Prx PAG. PAG and HBP have 96% of sequence identity to each other as previously noted (Figure 2A). The six residues that are different are distantly located from the active sites (Figure 2B). The solved structure of HBP is a homodimer. The monomer protein of HBP consists of four helices and six strands. Two monomers combine in the opposite direction to form a dimer. The active sites exist in symmetrical positions formed by Cys52 of A chain and Cys173 of B chain and vice versa. Our template structure is in an oxidized form, meaning that the cysteine residues form disulfide bonds.³¹ In the catalytic cycle of the peroxide-reducing action of Prx as shown in Figure 1, one might attempt to inhibit the reaction notated by the horizontal arm; however, this reaction will take place immediately after the previous reaction, in which S–H becomes S–OH. Therefore, one should start with the reduced form of the Prx dimer, even though the horizontal arm reaction is targeted. To predict the PAG structure of the reduced form, we simply broke the disulfide bonds and performed molecular dynamics on the resulting

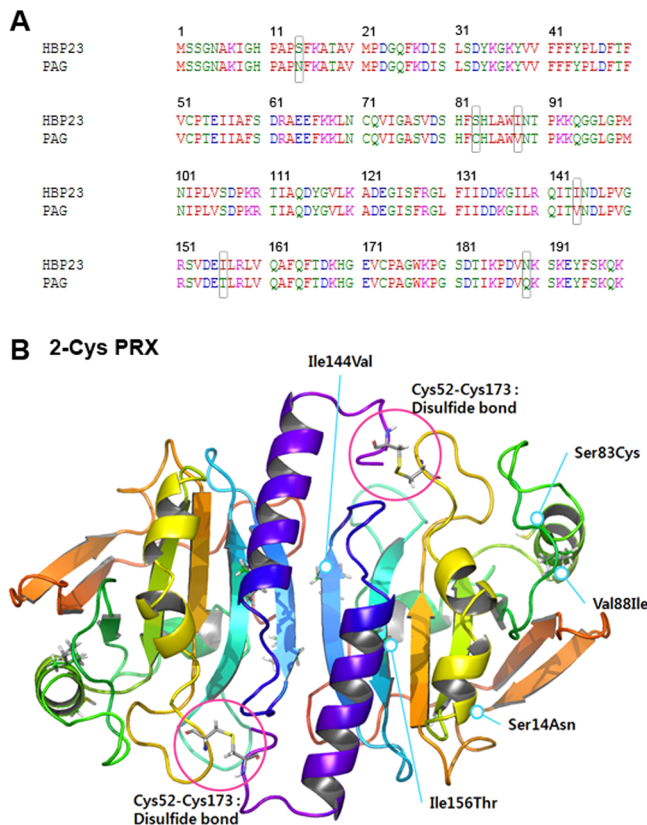


Figure 2. (A) Sequence comparison of 2 Cys HBP and 2-Cys PAG. (B) 2-Cys PAG structure predicted by homology modeling. Five of six residues that are different in two proteins are indicated. Because the residues numbered 176 and higher are missing from the template structure used (1QQ2), Gln189 was omitted from the predicted structure.

structure. We ran 40 ns of MD simulation. In Figure 3, a comparison can be found between the predicted oxidized-state structure (A) and the predicted reduced-state structure (B). With broken disulfide bonds, the two monomers tend to be loose, and there exists a larger hollow region between them, as depicted in red mesh.

Binding Sites of PAG. We ran SiteMap in search of possible binding sites on the surface of the modeled 2-Cys Prx PAG. SiteMap identified five primary binding sites as shown in Figure 4. Among these, the volume of site 1 was the largest. Two separate sites were identified near the active sites (sites 2 and 5); however, it seems difficult to fill up these sites to prevent a small molecule, such as H_2O_2 , to access the disulfide bridge site, because they are located on the sides of the disulfide bridge site. On the other hand, site 1 certainly seems druggable, with a groove large enough for drug-like molecules, which are typically in the range of 300–400 Da, to fit. Site 1 also has a mixture of hydrophilic and lipophilic residues surrounding it, which can provide adequate interaction points for a compound within it. The only problem with site 1 is that the entrance to it is narrow when Prx is in the oxidized state; however, our MD simulation for the reduced state of Prx showed that this entrance fluctuates, making the volume of site 1 at times reach a value more than 3 times that of the oxidized-state crystal structure form. Figure 5 shows the volume fluctuations of site 1 during MD simulation in both the reduced and oxidized states. After approximately 5 ns, although the volume of reduced state fluctuates rather wildly, it averages at a value definitely larger



Figure 3. Predicted structures of the (A) oxidized and (B) reduced states of 2-Cys PAG. The volumes of binding site 1 are depicted in red mesh.

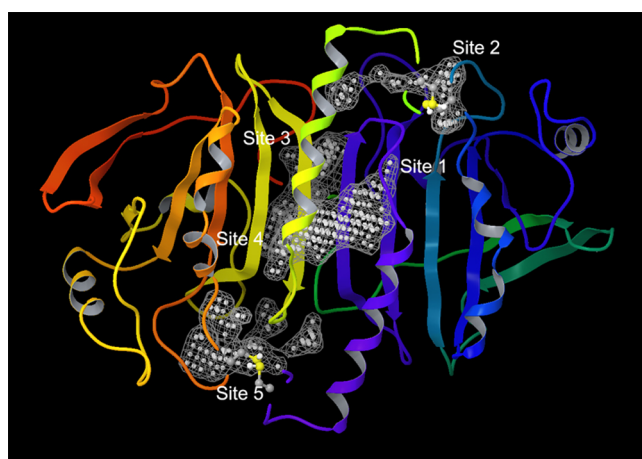


Figure 4. Predicted binding sites by SiteMap.

than the oxidized state. This result suggests that by controlling the fluctuation of site 1, one could influence the formation of disulfide bridges at the active sites.

Docking to Site 1. In order to find a way to control the volume fluctuation of site 1, we used a virtual ligand screening technique to discover a compound that would fit in this binding

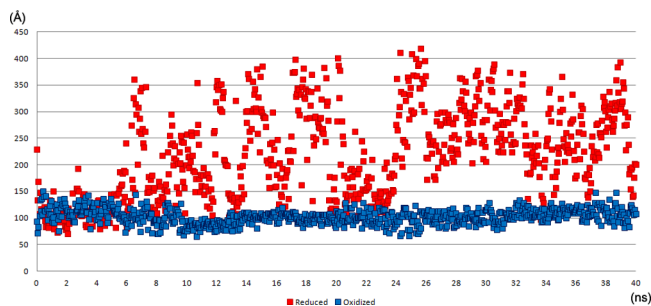


Figure 5. Plot of volumes of site 1 during MD simulation. The red and blue dots are for the reduced and oxidized states, respectively.

site. We screened ZINC virtual library using Glide SP mode with the Prx structure at 10 ns of MD simulation. After the structure reaches an equilibration point at approximately 5 ns in the MD simulation, even though there is quite a bit of fluctuation in the volume of the binding site, there is no appreciable change in conformation of the individual residues in the binding site, as confirmed by visual inspection of the trajectory files. Figure 6 shows the superposition of two

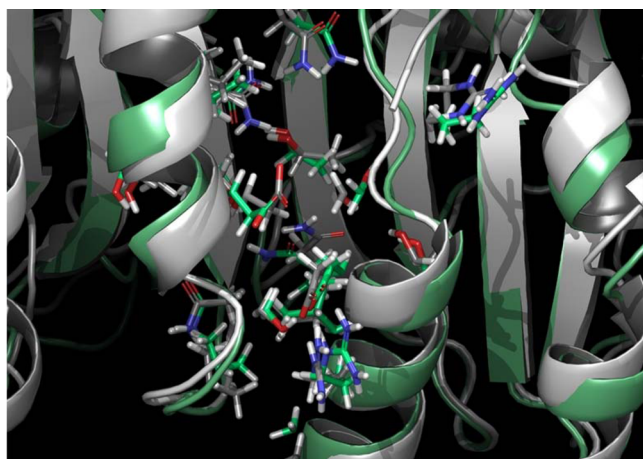


Figure 6. Superposition of the binding site 1 conformations at 15.05 and 7.95 ns of MD simulation.

conformations (at 15.05 and 7.95 ns) of the binding site. These conformations differ by 289 \AA^3 in volume, but this difference is mostly due to the fact that the gate to this binding site is floppy and that the volume calculation is greatly influenced by it. Therefore, the structure for docking was chosen at a point after equilibration at which the entrance to the binding site is wide open. Figure 7 shows the first-ranked compound from this screening with its interactions with surrounding residues. The compound is unmistakably drug-like and forms hydrogen bonds with residues GLU155(A), SER152(B), and THR156-(B) to give a high binding affinity (-9.87 kcal/mol). Although there were other compounds which yielded relatively high binding affinity, we used only the highest ranked compound in going forward, since we are not trying to produce an actual lead; rather, we are merely trying to demonstrate our concept of allosteric inhibition using modeling at this point and within the scope of this paper.

Subsequent MD Simulation for the Complex. With the compound found by docking in place, we ran MD simulations to observe the movement of the dimeric complex when the compound was set between the two monomers. Once the

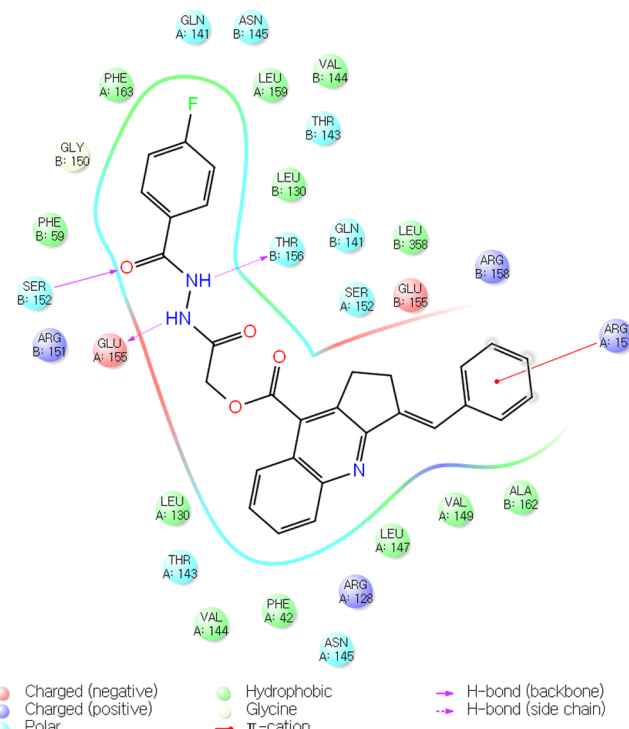


Figure 7. Interactions diagram of the top-ranked compound found by docking from the ZINC drug-like library with the surrounding residues.

compound was bound in the space between the two monomers, the pulsating motion of the dimer was reduced, and subsequently, the distance between the partnering cysteine residues (measured by the distance between 2 sulfur atoms) at each active site remained more or less constant at 10.35 \AA (standard deviation: 0.71 \AA) whereas, without the ligand, the distance fluctuated to a greater extent, and the average distance was smaller (6.95 \AA with standard deviation 1.19 \AA). Figure 8A

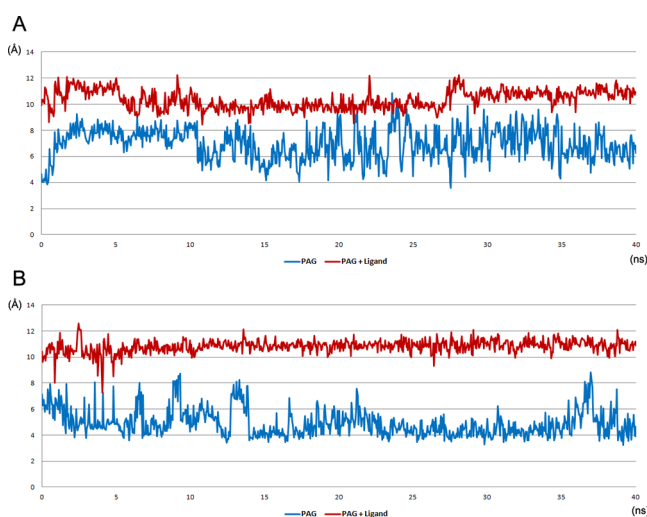


Figure 8. Plots of distances between sulfur atoms of partnering cysteine residues in the active site during MD simulations. The blue line indicates the case without a ligand, and the red line indicates the case with the ligand in site 1. (A) The reduced state of the Cys residues, and (B) the case when one of the Cys residues is oxidized to form $-\text{SOH}$.

shows the distance fluctuations of these two cases. Knowing that the length of a disulfide bond is approximately 2.05 Å, we can conclude that it would be virtually impossible to form such a bond when two sulfur atoms are rigidly fixed at a distance of 10.4 Å from each other. From the reduced state of the dimer, one of the pair of Cys residues can be oxidized to $-SOH$. When the compound is placed between the two monomers, the distance between $-SOH$ and $-SH$ would be still too far for dehydration to occur. The average distance of the sulfur atoms in this case is 10.82 Å, slightly larger than the reduced state, with standard deviation 0.49 Å, a more reduced value. On the other hand, without the ligand, the dimer tends to fluctuate just as wildly (standard deviation 1.03 Å) at an even smaller average value of Cys-Cys distance (4.92 Å). This means that without the ligand bound, once one of the Cys residues gets oxidized, the distance between sulfur atoms will get even smaller increasing the probability of disulfide-bond formation, whereas with the ligand bound, the distance remains constant at far enough a value that the probability of disulfide formation is very low. Figure 8B shows the distance between two Cys residues in this case. In conclusion, our MD simulation results show that it is much more likely that a disulfide bond would form without the ligand bound between the two monomers than with.

Free Energy Comparison. To determine whether the ligand binding is a thermodynamically more favorable reaction than the oxidization of the Prx dimer, we calculated end point free energies of the ligand and Prx dimer complex systems. We used MM/GBSA³² module of Prime³³ to calculate free energies of the ligand binding to the reduced form of the dimer and the oxidization process of the dimer. The free energy of the ligand binding is given by: $\langle G \rangle_{\text{ligand-reduced dimer complex}} - \langle G \rangle_{\text{ligand}}$ – $\langle G \rangle_{\text{reduced dimer}}$, whereas the free energy of the oxidization process is given by: $\langle G \rangle_{\text{oxidized dimer}} - \langle G \rangle_{\text{reduced dimer}}$, where G indicates Gibbs free energy.

The free energy of the ligand binding was –96.08 kcal/mol, while that of the oxidization of the reduced dimer was –75.69 kcal/mol. The ligand binding is more favorable, and therefore it is sensible to target the binding site between two monomers to inhibit the catalytic activity of Prx.

Proposed Mechanism of Inhibition. The result of MD simulation suggests that once the compound binds to the dimer Prx, the complex becomes stable and the distance between two cysteine residues remains large enough to significantly reduce the probability of the disulfide-bond formation. This simulated phenomenon can be used as a mechanism to inhibit Prx from being a reducing agent for H_2O_2 . If the cysteine residues are prevented from being near each other, H_2O_2 cannot be reduced; therefore, a compound that binds to the binding site located between two monomers of Prx can act as an inhibitor.

CONCLUSION

Recognizing that the space between two monomers of a dimeric Prx can be a druggable binding site, we used virtual ligand screening fueled by docking to discover a compound that could fit into this site and stabilize the fluctuation of the Prx dimer structure. Subsequent MD simulations revealed that when the discovered compound is bound, the fluctuation of the complex structure is reduced such that the distance between cysteine residues is kept constant at a value exceeding the threshold for disulfide-bond formation. This mechanism can be used for allosteric inhibition of Prx as a reducing agent for H_2O_2 . The finding suggests that the binding site between two

monomers can be a target for an anticancer drug discovery, following the proposed use of inhibition of Prx for such a pharmaceutical interest. We believe that there could be more cases in which such a mechanism works as an allosteric inhibition for dimeric enzymes, because disturbing the aggregation of two monomers can bring about a structural change of the dimer, which in turn, can disrupt the enzymatic function. Further research along the same line is certainly warranted as well as experimental verification of the theoretical hypothesis.

AUTHOR INFORMATION

Corresponding Author

*E-mail: artcho@korea.ac.kr

Notes

The authors declare no competing financial interest.

ACKNOWLEDGMENTS

We thank Schrödinger LLC (Portland, OR, U.S.A.) for the generous supply of the software used for this research. This work was supported by the National Research Foundation of Korea (NRF) grant (grant no. 2012043211).

REFERENCES

- (1) Forman, H. J. Introduction to serial reviews on peroxiredoxins. *Free Radical Biol. Med.* **2005**, *38*, 1411–1412.
- (2) Lehtonen, S. T.; Svensk, A. M.; Soini, Y.; Paakkko, P.; Hirvikoski, P.; Kang, S. W.; Saily, M.; Kinnula, V. L. Peroxiredoxins, a novel protein family in lung cancer. *Int. J. Cancer* **2004**, *111*, 514–521.
- (3) Wood, Z. A.; Schroder, E.; Harris, J. R.; Poole, L. B. Structure, mechanism and regulation of peroxiredoxins. *Trends Biochem. Sci.* **2003**, *28*, 32–40.
- (4) Rahman, I.; Biswas, S. K.; Kode, A. Oxidant and antioxidant balance in the airways and airway diseases. *Eur. J. Pharmacol.* **2006**, *533*, 222–239.
- (5) Bagnall, N. H.; Kotze, A. C. cDNA cloning and expression patterns of a peroxiredoxin, a catalase and a glutathione peroxidase from *Haemonchus contortus*. *Parasitology Res.* **2004**, *94*, 283–289.
- (6) Immenschuh, S.; Baumgart-Vogt, E. Peroxiredoxins, oxidative stress, and cell proliferation. *Antioxid. Redox Signaling* **2005**, *7*, 768–777.
- (7) Hofmann, B.; Hecht, H. J.; Flohé, L. Peroxiredoxins. *Biol. Chem.* **2002**, *383*, 347–364.
- (8) Seo, M. S.; Kang, S. W.; Kim, K.; Baines, I. C.; Lee, T. H.; Rhee, S. G. Identification of a new type of mammalian peroxiredoxin that forms an intramolecular disulfide as a reaction intermediate. *J. Biol. Chem.* **2000**, *275*, 20346–20354.
- (9) Choi, H. J.; Kang, S. W.; Yang, C. H.; Rhee, S. G.; Ryu, S. E. Crystal structure of a novel human peroxidase enzyme at 2.0 angstrom resolution. *Nat. Struct. Biol.* **1998**, *5*, 400–406.
- (10) Hirotsu, S.; Abe, Y.; Okada, K.; Nagahara, N.; Hori, H.; Nishino, T.; Hakoshima, T. Crystal structure of a multifunctional 2-Cys peroxiredoxin heme-binding protein 23 kDa/proliferation-associated gene product. *Proc. Natl. Acad. Sci. U.S.A.* **1999**, *96*, 12333–12338.
- (11) Schroder, E.; Littlechild, J. A.; Lebedev, A. A.; Errington, N.; Vagin, A. A.; Isupov, M. N. Crystal structure of decameric 2-Cys peroxiredoxin from human erythrocytes at 1.7 angstrom resolution. *Structure* **2000**, *8*, 605–615.
- (12) Nogoceke, E.; Gommel, D. U.; Kiess, M.; Kalisz, H. M.; Flohé, L. A unique cascade of oxidoreductases catalyses trypanothione-mediated peroxide metabolism in *Cryptosporidium fasciculata*. *Biol. Chem.* **1997**, *378*, 827–836.
- (13) Poole, L. B.; Reynolds, C. M.; Wood, Z. A.; Karplus, P. A.; Ellis, H. R.; Calzi, M. L. AhpF and other NADH: peroxiredoxin oxidoreductases, homologues of low M-r thioredoxin reductase. *Eur. J. Biochem.* **2000**, *267*, 6126–6133.

- (14) Bryk, R.; Lima, C. D.; Erdjument-Bromage, H.; Tempst, P.; Nathan, C. Metabolic enzymes of mycobacteria linked to antioxidant defense by a thioredoxin-like protein. *Science* **2002**, *295*, 1073–1077.
- (15) Behrend, L.; Henderson, G.; Zwacka, R. M. Reactive oxygen species in oncogenic transformation. *Biochem. Soc. Trans.* **2003**, *31*, 1441–1444.
- (16) Noh, D. Y.; Ahn, S. J.; Lee, R. A.; Kim, S. W.; Park, I. A.; Chae, H. Z. Overexpression of peroxiredoxin in human breast cancer. *Anticancer Res.* **2001**, *21*, 2085–2090.
- (17) Park, J. H.; Kim, Y. S.; Lee, H. L.; Shim, J. Y.; Lee, K. S.; Oh, Y. J.; Shin, S. S.; Choi, Y. H.; Park, K. J.; Park, R. W.; Hwang, S. C. Expression of peroxiredoxin and thioredoxin in human lung cancer and paired normal lung. *Respirology* **2006**, *11*, 269–275.
- (18) Bae, J. Y.; Ahn, S. J.; Han, W.; Noh, D. Y. Peroxiredoxin I and II inhibit H₂O₂-induced cell death in MCF-7 cell lines. *J. Cell. Biochem.* **2007**, *101*, 1038–1045.
- (19) Wang, T.; Tamae, D.; LeBon, T.; Shively, J. E.; Yen, Y.; Li, J. J. The role of peroxiredoxin II in radiation-resistant MCF-7 breast cancer cells. *Cancer Res.* **2005**, *65*, 10338–10346.
- (20) Schumacker, P. T. Reactive oxygen species in cancer cells: live by the sword, die by the sword. *Cancer Cell* **2006**, *10*, 175–176.
- (21) Trachootham, D.; Zhou, Y.; Zhang, H.; Demizu, Y.; Chen, Z.; Pelicano, H.; Chiao, P. J.; Achanta, G.; Arlinghaus, R. B.; Liu, J.; Huang, P. Selective killing of oncogenically transformed cells through a ROS-mediated mechanism by beta-phenylethyl isothiocyanate. *Cancer Cell* **2006**, *10*, 241–252.
- (22) Christopoulos, A.; May, L. T.; Avlani, V. A.; Sexton, P. M. G-protein-coupled receptor allosterism: the promise and the problem(s). *Biochem. Soc. Trans.* **2004**, *32*, 873–877.
- (23) May, L. T.; Avlani, V. A.; Sexton, P. M.; Christopoulos, A. Allosteric modulation of G protein-coupled receptors. *Curr. Pharm. Des.* **2004**, *10*, 2003–2013.
- (24) Chae, H. Z.; Kim, H. J.; Kang, S. W.; Rhee, S. G. Characterization of three isoforms of mammalian peroxiredoxin that reduce peroxides in the presence of thioredoxin. *Diabetes Res. Clin. Pract.* **1999**, *45*, 101–112.
- (25) Weichsel, A.; Gasdaska, J. R.; Powis, G.; Montfort, W. R. Crystal structures of reduced, oxidized, and mutated human thioredoxins: evidence for a regulatory homodimer. *Structure* **1996**, *4*, 735–751.
- (26) Choi, H. J.; Kang, S. W.; Yang, C. H.; Rhee, S. G.; Ryu, S. E. Crystal structure of a novel human peroxidase enzyme at 2.0 Å resolution. *Nat. Struct. Biol.* **1998**, *5*, 400–406.
- (27) Bordoli, L.; Kiefer, F.; Arnold, K.; Benkert, P.; Battey, J.; Schwede, T. Protein structure homology modeling using SWISS-MODEL workspace. *Nat. Protoc.* **2009**, *4*, 1–13.
- (28) Halgren, T. A. Identifying and Characterizing Binding Sites and Assessing Druggability. *J. Chem. Inf. Model.* **2009**, *49*, 377–389.
- (29) Chung, J. Y.; Hah, J. M.; Cho, A. E. Correlation between performance of QM/MM docking and simple classification of binding sites. *J. Chem. Inf. Model.* **2009**, *49*, 2382–2387.
- (30) Irwin, J. J.; Shoichet, B. K. ZINC-a free database of commercially available compounds for virtual screening. *J. Chem. Inf. Model.* **2005**, *45*, 177–182.
- (31) Chae, H. Z.; Uhm, T. B.; Rhee, S. G. Dimerization of thiol-specific antioxidant and the essential role of cysteine 47. *Proc. Natl. Acad. Sci. U.S.A.* **1994**, *91*, 7022–7026.
- (32) Parenti, M. D.; Rastelli, G. Advances and applications of binding affinity prediction methods in drug discovery. *Biotechnol. Adv.* **2012**, *30*, 244–250.
- (33) Du, J.; Sun, H.; Xi, L.; Li, J.; Yang, Y.; Liu, H.; Yao, X. Molecular modeling study of checkpoint kinase 1 inhibitors by multiple docking strategies and prime/MM-GBSA calculation. *J. Comput. Chem.* **2011**, *32*, 2800–2809.